

A Burst and Simultaneous Short-Term Pulsed Flux Enhancement from the Magnetar Candidate 1E 1048.1–5937

Fotis P. Gavriil, Victoria M. Kaspi

*Department of Physics, Rutherford Physics Building, McGill University, 3600 University
Street, Montreal, Quebec, H3A 2T8, Canada*

and

Peter M. Woods¹

*Space Science Research Center, National Space Science and Technology Center, Huntsville,
AL 35805, USA*

ABSTRACT

We report on the 2004 June 29 X-ray burst detected from the direction of the Anomalous X-ray Pulsar (AXP) 1E 1048.1–5937 using the *Rossi X-ray Timing Explorer (RXTE)*. We find a simultaneous increase of ~ 3.5 times the quiescent value in the 2–10 keV pulsed flux of 1E 1048.1–5937 during the tail of the burst which identifies the AXP as the burst’s origin. The burst was overall very similar to the two others reported from the direction of this source in 2001. The unambiguous identification of 1E 1048.1–5937 as the burster here confirms it was the origin of the 2001 bursts as well. The epoch of the burst peak was very close to the arrival time of 1E 1048.1–5937’s pulse peak. The burst exhibited significant spectral evolution with the trend going from hard to soft. Although the average spectrum of the burst was comparable in hardness ($\Gamma \sim 1.6$) to those of the 2001 bursts, the peak of this burst was much harder ($\Gamma \sim 0.3$). During the 11 days following the burst, the AXP was observed further with *RXTE*, *XMM-Newton* and *Chandra*. Pre- and post-burst observations revealed no change in the total flux or spectrum of the quiescent emission. Comparing all three bursts detected thus far from this source we find that this event was the most fluent ($> 3.3 \times 10^{-8}$ erg cm⁻² in the 2–20 keV band), had the highest peak flux ($59 \pm 9 \times 10^{-10}$ erg s⁻¹ cm⁻² in the 2–20 keV band), and the longest duration (> 699 s). The long duration of the burst differentiates it from Soft Gamma Repeater (SGR) bursts which have

¹Universities Space Research Association

typical durations of ~ 0.1 s. Bursts that occur preferentially at pulse maximum, have fast-rises and long X-tails containing the majority of the total burst energy have been seen uniquely from AXPs. The marked differences between AXP and SGRs bursts may provide new clues to help understand the physical differences between these objects.

Subject headings: pulsars: general — pulsars: individual (1E 1048.1–5937) — X-rays: bursts

1. Introduction

The nature of the source class colloquially known as Anomalous X-ray Pulsars (AXPs) has been well explained by the so called magnetar model (Thompson & Duncan 1996). In this model, AXPs, which appear to be isolated, have pulse periods in the narrow range of 5–12 s, and X-ray luminosities which greatly exceed their spin-down luminosities, are young, isolated, ultra-magnetized neutron stars which are powered by their decaying magnetic fields. The magnetar model was first introduced to explain the enigmatic properties of the Soft Gamma Repeaters (SGRs). The SGRs were first identified by their emission of long-lived super-Eddington flares in soft γ -rays and by their much more frequent and less energetic short bursts in hard X-rays (Mazets et al. 1979; Hurley et al. 1999). Since their discovery, the quiescent emission of SGRs has been shown to possess numerous similarities with the persistent emission of AXPs. Specifically, the SGRs were shown to have similar pulse periods and spin down rates (Kouveliotou et al. 1998; Kouveliotou et al. 1999). For a recent review of AXPs and SGRs see Woods & Thompson (2004).

The distinction between AXPs and SGRs was blurred even further when the *Rossi X-ray Timing Explorer (RXTE)* discovered two magnetar-like X-rays bursts from the direction of AXP 1E 1048.1–5937 (Gavriil et al. 2002). The temporal, energetic and spectral properties of these bursts were very similar to those of SGRs. Due to the large field of view of *RXTE*, the AXP could not be unambiguously confirmed as the source of the bursts, however the burst properties argued strongly that the AXP was indeed the origin. The issue of whether AXPs emit bursts was settled unambiguously when another AXP, 1E 2259+586, underwent a major SGR-like outburst involving 80 bursts accompanied by severe changes to every aspect of the pulsed emission (Kaspi et al. 2003; Woods et al. 2004). The distribution of durations and fluences of these bursts were very similar to the ones seen in SGRs (Gavriil et al. 2004). Despite the many similarities between SGR and AXP bursts, there were some differences. For instance, the first burst detected from the direction of 1E 1048.1–5937 exhibited an unusual spectral feature near ~ 14 keV during the first ~ 1 s of the burst. Furthermore, in

AXPs the more luminous bursts had harder spectra, the opposite of what is seen in SGRs.

Besides being able to account for the quiescent emission of SGRs and AXPs, the magnetar model provides a clear explanation for the bursts (Thompson & Duncan 1995). The highly twisted interior magnetic fields of a magnetar diffuses out and unwinds, causing enormous stresses on the neutron star’s crust. When the crust yields to these internal stresses, the well anchored foot-points of the external field are displaced, sending electromagnetic disturbances, i.e. Alfvén waves into the magnetosphere. The Alfvén waves provide the energy and momentum required for photons in the magnetosphere to pair-produce, yielding an electron-positron and photon fireball. This fireball is contained by closed field lines, and is gradually radiated away. The magnetic field strengths required to contain the energy released in SGR bursts are consistent with the dipolar field strengths inferred from their spin-down (Kouveliotou et al. 1998; Kouveliotou et al. 1999).

We report here, using data from our continuing *RXTE* monitoring program, the discovery of another X-ray burst from AXP 1E 1048.1–5937. We show that the pulsed emission increased in the tail of the burst, indicating that the AXP was unambiguously the source of the burst. The identification of 1E 1048.1–5937 as the burst source for this event and the similarities between this burst and the previous two lends further support to the AXP having also been the emitter of the two bursts reported by Gavriil et al. (2002).

2. Results

2.1. *RXTE* Observations

The results presented here were obtained using the Proportional Counter Array (PCA; Jahoda et al. 1996) on board *RXTE*. The PCA consists of an array of five collimated xenon/methane multi-anode proportional counter units (PCUs) operating in the 2–60 keV range, with a total effective area of approximately 6500 cm² and a field of view of $\sim 1^\circ$ FWHM. We use *RXTE* to monitor all five known AXPs on a regular basis as part of a long-term monitoring campaign (see Gavriil & Kaspi 2002, and references therein). On 2004 June 29, during one of our regular monitoring observations (*RXTE* observation identification 90076-02-09-02) that commenced at UT 06:29:28, the AXP 1E 1048.1–5937 exhibited an SGR-like burst.

2.1.1. Burst Search

The burst was identified using the burst searching algorithm introduced in Gavriil et al. (2002) and described in detail in Gavriil et al. (2004). To summarize briefly, time series were created separately for each PCU using all xenon layers. Light curves with time bin widths of 1/32 s were created. The FT00Ls `xtfilt` and `maketime` were used to determine the intervals over which each PCU was off. We further restricted the data set by including only events in the energy range 2–20 keV. Time bins with significant excursions from a running mean were flagged and subject to further investigation. The observation had total on-source integration time of 2.0 ks. There were exactly three PCUs operational at all times and the burst was equally significant in all three PCUs. Data were collected in the `GoodXenonwithPropane` mode, which records the arrival time (with 1- μ s resolution) and energy (with 256-channel resolution) of every unrejected xenon event as well as all the propane layer events. Photon arrival times were adjusted to the solar system barycenter using a source position of (J2000) RA = 10^h 50^m 07^s.12, DEC = –59°53′21″.37 (Israel et al. 2002) and the JPL DE200 planetary ephemeris. Note that following the burst we initiated a 20.2 ks long *RXTE*/PCA Target of opportunity (ToO) observation on 2004 July 8. Similarly, on 2004 July 10, we initiated 3 more *RXTE*/PCA ToO observations which had integration times of 3.6 ks, 15.0 ks and 20.2 ks respectively. No more bursts or other unusual behavior were seen in the ToO observations or in any of the monitoring observations since the burst.

2.1.2. Burst Temporal Properties

We analyzed the temporal properties of the burst in order to compare them to those of other bursts from AXPs and SGRs. The analysis methods are explained in greater detail elsewhere (e.g., see Gavriil et al. 2002, 2004; Woods et al. 2005) The burst profile is shown in Figure 1 and its measured properties are summarized in Table 1. The burst peak time was initially defined, using a time series binned with 1/32 s resolution, as the midpoint of the bin with the highest count rate. We redefined this value, using the event timestamps within this time bin, as the midpoint of the two events having the shortest separation.

Using the burst peak time, we determined the occurrence of the burst in pulse phase. We split our observation into four segments and phase-connected these intervals using the burst peak time as our reference epoch. We then folded our data using the resulting ephemeris and cross-correlated our folded profile with a high signal-to-noise template whose peak was centered on phase $\phi = 0$, where ϕ is measured in cycles. (For a review of our timing techniques, see Kaspi et al. 1999, 2000, 2001; Gavriil & Kaspi 2002). We find that the burst occurred near the peak of 1E 1048.1–5937’s pulse profile, at $\phi = -0.078 \pm 0.016$.

The burst rise time was determined by a maximum likelihood fit to the unbinned data using a piecewise function having a linear rise and exponential decay. The burst rise time, t_r , was defined as the time from the peak to when the linear component reached the background (§ 2.1.4 discusses how the background was estimated). The burst duration, T_{90} , is the interval between when 5% and 95% of the total 2–20 keV burst fluence was received. As we will note in § 2.1.4, the burst did not fade away before the end of our observation. Thus we could only place an upper limit of > 699 s on the burst duration, which is the time from the burst’s peak to the end of our observation. This very long tail can be seen in the burst profile in Figure 1, which shows a significant excess from the burst’s peak to the end of our observation.

2.1.3. Burst Spectral Evolution

Significant spectral evolution has been noted for the first burst discovered from this source (Gavriil et al. 2002) as well as for bursts from AXP XTE J1810–197 (Woods et al. 2005) and bursts from SGRs (Ibrahim et al. 2001; Lenters et al. 2003). Motivated by these observations we extracted spectra at different intervals within the burst’s duration. We increased the integration time of the spectra as we went further away from the burst to maintain adequate signal-to-noise. A background spectrum was extracted from a 1000-s long interval which ended 10 s before the burst. From each of the burst intervals and the background interval we subtracted the instrumental background as estimated from the tool `pcabackest`. Each burst interval spectrum was grouped so that there were never fewer than 20 counts per spectral bin after background subtraction. The regrouped spectra along with their background estimators were used as input to the X-ray spectral fitting software package `XSPEC`¹. Response matrices were created using the FT00Ls `xtfilt` and `pcarsp`. All channels below 2 keV and above 30 keV were ignored leaving 10–24 spectral bins for fitting. We fit the burst spectra to a photoelectrically absorbed blackbody model which adequately characterized the data. In all fits, the column density was held fixed at the average value of our *Chandra* and *XMM-Newton* observations (see § 2.2.2 and Table 2). The burst’s bolometric flux, blackbody temperature and radius evolution are shown in Figure 1. The bolometric flux decayed as a power law in time, $F = F_1(t/1 \text{ s})^\beta$, where $F_1 = 1.84 \pm 0.36 \times 10^{-8} \text{ erg cm}^{-2} \text{ s}^{-1}$ and $\beta = -0.82 \pm 0.05$. The blackbody temperature decayed as $kT = kT_1 - \alpha \log(t/1 \text{ s})$, where $kT_1 = 6.24 \pm 0.71 \text{ keV}$ and $\alpha = 1.55 \pm 0.41 \text{ keV}$. The blackbody emission radius remained relatively flat with an average value of $R = 0.100 \pm 0.01 \text{ km}$. The blackbody radius was calculated assuming a distance of 5 kpc to the source. We repeated the above procedure using a power-law model, which also adequately characterized the data.

¹<http://xspec.gsfc.nasa.gov>

Our power-law spectral index time series is shown in Figure 1, where we see that the initial spike of the burst is very hard, with the burst gradually softening as the flux decays. Fitting a logarithmic function to the power-law spectral index time series we find $\Gamma = \Gamma_1 + \alpha \log(t/1 \text{ s})$, where $\Gamma_1 = 0.30 \pm 0.18$ and $\alpha = 0.39 \pm 0.13$.

Possible spectral features have been reported in bursts from AXPs 1E 1048.1–5937 (Gavriil et al. 2002) and XTE J1810–197 (Woods et al. 2005) and from bursts from two SGRs (Strohmayer & Ibrahim 2000; Ibrahim et al. 2002, 2003). We searched for features by extracting spectra of different integration times as was done for the spectral evolution analysis. The spectra were background-subtracted and grouped in the exact same fashion as in the spectral evolution analysis. Energies below 2 keV and above 30 keV were ignored, leaving 13 spectral channels for fitting. Regrouped spectra, background estimators and response matrices were fed into XSPEC. Spectra were fit with a photoelectrically absorbed blackbody model, holding only N_H fixed at the same value used in the spectral evolution analysis. The first 8 s of the burst spectrum was poorly fit by a continuum model, because of significant residuals centered near 13 keV. The apparent line feature was most significant if the first second of the burst was excluded. A simple blackbody fit had reduced $\chi^2_{\text{dof}} = 1.61$ for 11 degrees of freedom (see Figure 3). The probability of obtaining such a value of χ^2 or larger under the hypothesis that the model is correct is very low, $P(\chi^2 \geq 17.75) = 0.088$. The fit was greatly improved by the addition of a Gaussian emission line; in this case the fit had $\chi^2_{\text{dof}} = 0.56$ for 8 degrees of freedom (see Figure 3). The probability of obtaining such a value of χ^2 or larger under the hypothesis that the model is correct is $P(\chi^2 \geq 4.75) = .784$. The line energy was $E = 13.09 \pm 0.25$ keV. Note that a line at a similar energy was found by Gavriil et al. (2002) in the first burst discovered from this source.

To firmly establish the significance of this feature, we performed the following Monte Carlo simulation in XPSEC. We generated 10000 fake spectra drawn from a simple blackbody model having the same background and exposure as our data set. We fit the simulated data to a blackbody model and to a blackbody plus emission line model and compared the χ^2 difference between the two. To ensure we were sensitive to narrow lines when fitting our blackbody plus emission line model we stepped through different line energies from 2 to 30 keV in steps of 0.2 keV and refit our spectrum holding the line energy fixed and recorded the lowest χ^2 value returned. In our simulations only 11 events had a χ^2 difference greater or equal to the one found from our data. Thus, the probability of obtaining a spectral feature of equal significance by random chance is ~ 0.0011 . The significance of the spectral feature reported for this source by Gavriil et al. (2002) at this energy was ~ 0.0008 . Since these were independent measurements, the probability of finding two spectral features at the same energy by random chance is $\sim 8.8 \times 10^{-7}$, thus the emission line at ~ 13 keV is genuine.

2.1.4. Burst Energetics

In order to compare the energetics of this burst to those emitted in 2001 we measured its peak flux and fluence. The first step in this analysis was to model the background count rate. First we extracted an instrumental background for the entire observation using `pcabackest`. The function `pcabackest` can only estimate the background rate every 16 s seconds, so we interpolated to finer resolution by modeling the background rate as a 5th order polynomial. We then added the average non-burst count rate to this model. We estimated this value by subtracting our interpolated `pcabackest` model from our data and then measuring the average count rate over the same interval used to estimate the background in the spectral evolution analysis. The 2–20 keV peak flux was determined from the event data using a box-car integrator of width $1/\Delta t$. We used $\Delta t = 64$ ms and $\Delta t = t_r$ (for details on the flux calculation algorithm, see Gavriil et al. 2004). At each step of the boxcar we subtracted the total number of background counts as determined by integrating our background model over the boxcar limits. To convert our flux measurements from count rates to CGS units we extracted spectra whose limits were defined by the start and stop time of the boxcars. For each flux measurement we extracted a spectrum for the region of interest, a background spectrum and a response matrix, similar to what was done for the spectral evolution analysis. Each spectrum was fit to a photoelectrically absorbed blackbody using `XSPEC` in order to measure the 2–20 keV flux in CGS units. The 2–20 keV total fluence was determined by integrating our background-subtracted time series. If the burst had emitted all of its energy during the observation, the integrated burst profile would eventually plateau. However, this is not what we observed. The integrated burst profile was still steadily rising even at the end of our observation, indicating that our observation finished before catching the end of the burst. Thus, we can only set an upper-limit on the total 2–20 keV fluence; see Table 1. To convert our fluence upper limit from counts to CGS units the exact procedure was followed as for the peak flux measurements.

2.1.5. Pulsed Flux Measurements

Magnetar candidates have been observed to be highly flux variable, which is why we regularly monitor the pulsed flux of this source (see Gavriil & Kaspi 2004, for a detailed discussion of pulsed flux calculations for 1E 1048.1–5937). The pulsed flux during the entire observation in which the burst occurred was not significantly higher than in neighboring observations. However, in some AXPs and SGRs, short time-scale ($\ll 1000$ s) abrupt changes in pulsed flux have been observed in conjunction with bursts (e.g. Lenters et al. 2003; Woods et al. 2004, 2005). Motivated by such observations we decided to search for short-term

pulsed flux enhancements around the time of the burst from 1E 1048.1–5937. We broke the observation into 10 intervals and calculated the pulsed flux for each. In order to avoid having the burst spike biasing our pulsed flux measurements we removed a 4 s interval centered on the burst peak. A factor of 3.5 increase in pulsed flux can be seen in the tail of the burst (see Fig. 2). This coupling between bursting activity and pulsed flux establishes that 1E 1048.1–5937 is definitely the burst source.

2.2. Imaging X-ray Observations

Following the discovery of a new burst from the direction of 1E 1048.1–5937, we triggered observations of the source with imaging X-ray telescopes. The AXP was observed once with *XMM-Newton* on 2004 July 8 for 33 ks and twice with *Chandra* on 2004 July 10 and 15 for 29 and 28 ks, respectively. Simultaneous *RXTE* observations were performed during the *XMM-Newton* and the first *Chandra* observation to assist in the identification of bursts. For scheduling reasons the second *Chandra* observation could not be coordinated with simultaneous *RXTE* observations.

The *XMM-Newton* data were processed using the *XMM-Newton* Science Analysis System² (SAS) v6.0.0. The scripts `epchain` and `emchain` were run on the Observation Data Files for the PN and MOS data, respectively. For the *Chandra* data, we started from the filtered event 2 list for all results presented here. Standard analysis threads were followed to extract filtered event lists, light curves and spectra from the processed data. See below for more details. The approximate count rates for the *XMM-Newton* PN observation was 2.69 ± 0.01 counts s^{-1} in the 0.5–12 keV band. The first and second *Chandra* observation had a count rate of 1.344 ± 0.007 counts s^{-1} and 1.302 ± 0.007 counts s^{-1} , respectively, in the 0.5–10 keV band.

2.2.1. Burst Search

The *XMM-Newton* PN camera and *Chandra* ACIS detectors (S3 chip) were operated in similar modes (`TIMING` for PN and `CC mode` for ACIS) to optimize the time resolution in order to search for short X-ray bursts (5.96 ms for PN and 2.85 ms for ACIS). Filtered source event lists (0.5–12.0 keV for PN and 0.5–10.0 keV for ACIS) were extracted for each observation to create light curves at three different time resolutions: 1, 10 and 100 times

²http://xmm.vilspa.esa.es/external/xmm_sw_cal/sas.shtml

the nominal time resolution of the data. No bursts were found in any of the light curves. Moreover, no bursts were seen within the *RXTE* PCA data of the simultaneous observations of 1E 1048.1–5937. Aside from the regular X-ray pulsations, the intensity of 1E 1048.1–5937 does not vary significantly within these observations.

2.2.2. Persistent Emission Properties

Motivated by the sometimes dramatic changes in the persistent, pulsed X-ray emission of SGRs and AXPs following burst activity (e.g. Woods et al. 2004), we investigated both the spectral and temporal properties of the X-ray emission from 1E 1048.1–5937 using the *XMM-Newton* and *Chandra* data. Admittedly, only a single, relatively weak burst was observed from 1E 1048.1–5937 on 2004 June 29, so significant changes in these properties are not necessarily expected. However, this particular source has shown significant variability in its pulsed flux and pulsed fraction over the last several years apparently independent of strong burst activity (Gavriil & Kaspi 2004; Mereghetti et al. 2004), so searching for continued evolution in these properties is of interest.

The **TIMING** mode for PN data is not yet well calibrated for spectral analysis, so we accumulated a spectrum from the MOS1 camera which was operated in **SMALL WINDOW** mode. The source spectrum was extracted from a circular region centered on the AXP with a radius of 35". A background spectrum was extracted from a circular (radius = 80"), source free region on CCD #3, closest to the center of the field of view. The calibration files used to generate the effective area file and response matrix were downloaded on 2004 August 3. The source spectrum was grouped to contain no fewer than 25 counts per channel and fit using **XSPEC**. We obtained a satisfactory fit to the energy spectrum (0.3–12.0 keV) using the standard blackbody plus power-law (BB+PL) model. Fit parameters are given in Table 2.

For the *Chandra* observations, source spectra were extracted from a rectangular region centered on the source with a dimension along the ACIS-S3 readout direction of 16 pixels ($\sim 8''$). Background spectra were extracted from 40 pixel wide rectangular regions on either side of the source with a gap of 7 pixels in between the source and background regions. Effective area files and response matrices were generated using CALDB v2.23. Similar to the *XMM-Newton* spectral analysis, the *Chandra* spectra were grouped and fit to the BB+PL model. We were unable to obtain a satisfactory fit to either *Chandra* data set due to the presence of an emission line at 1.79 keV. This feature is instrumental in origin caused by an excess of Silicon fluorescence photons recorded in the CCD (?). To avoid this feature and calibration uncertainties between 0.3 and 0.5 keV that give rise to large residuals in this range, we restricted our spectral fits to 0.5–1.67 and 1.91–10.0 keV. See Table 2 for fit

parameters.

Using the PN data from *XMM-Newton* and the ACIS data from *Chandra*, we measured the root-mean-square (rms) pulsed fraction of 1E 1048.1–5937 during each of the three observations for different energy bands. For the PN data, a source event list was extracted from a 5.6 pixel wide rectangular region centered on the AXP³ and the times were corrected to the solar system barycenter. A background event list was extracted from two 10 pixel wide rectangles on either side of the source with a 10 pixel gap between the source and background regions. The same source and background regions used for the spectral analysis of the *Chandra* data were used here for the pulse timing analysis. The *Chandra* photon arrival times were corrected for instrumental time offsets⁴ and to the solar system barycenter. Best-fit frequencies were measured independently for each observation and found to be consistent with the more precise *RXTE* spin ephemeris. We constructed background-subtracted folded pulse profiles for each observation for different energy ranges and measured the rms pulsed fraction following Woods et al. (2004) using the Fourier power from the first 3 harmonics. The pulsed fraction increases with energy from $46.6 \pm 0.5\%$ in the 0.5–1.7 keV range to $56.8 \pm 1.0\%$ in the 3.0–7.0 keV range. The 2.0–10.0 keV pulsed fractions are listed in Table 2.

Comparing our results to those of Mereghetti et al. (2004), we find that both the flux and the pulsed fraction are intermediate between the *XMM-Newton* observations in 2000 December and 2003 June (Figure 4). The definition of pulsed fraction introduced by Mereghetti et al. (2004) is significantly different than ours. Therefore, we analyzed each of the archival *XMM-Newton* data sets for this source in the same manner as described above for the 2004 data set. Similar to the behavior seen in 2004, we find that the pulsed fraction increases significantly with energy within each archival data set. The average pulsed fractions during these observations, however, are significantly different than in 2004. We measure rms pulsed fractions (2.0–10.0 keV) of $76.0 \pm 2.3\%$ and $43.9 \pm 0.4\%$ for the respective observations. The observation in 2000 took place well before the onset of the first pulsed flux flare (Gavriil & Kaspi 2004) and the two bursts seen near the peak of that flare (Gavriil et al. 2002). The observation in 2003 took place during the decay of the second flare which peaked one year earlier. We conclude that both the flux and pulsed fraction that changed so drastically during these extended flares appear to be returning to their “nominal” pre-flare levels. It is interesting to note that the pulsed fraction decreases during these flares showing a possible anti-correlation with the phase-averaged flux. Thus, the relative increase in the phase-averaged flux is actually much larger than the increase in pulsed flux seen in

³http://wave.xray.mpe.mpg.de/xmm/cookbook/EPIC_PN/timing/timing_mode.html

⁴<http://wwwastro.msfc.nasa.gov/xray/ACIS/cctime/>

the *RXTE*/PCA light curve (i.e. the phase-averaged flux time history may have exhibited a stronger peak).

3. Discussion

We have discovered the longest, most luminous and most energetic burst from 1E 1048.1–5937 thus far. The short-term pulsed flux enhancement at the time of the burst establishes that 1E 1048.1–5937 is definitely the burst source and in all likelihood was the source of the 2001 bursts as well.

An interesting property of all three bursts from 1E 1048.1–5937 is that they occur preferentially at pulse maximum. A similar trend was found for the transient AXP XTE J1810–197 for which four bursts occurred near pulse maximum (Woods et al. 2005). Furthermore, in a major outburst from AXP 1E 2259+586 involving ~ 80 bursts, Gavriil et al. (2004) found that bursts occurred preferentially at pulse phases for which the pulsed emission was high (note that the pulse profile of 1E 2259+586 is double-peaked as opposed to the quasi-sinusoidal profiles of 1E 1048.1–5937 and XTE J1810–197, see Gavriil & Kaspi 2002). SGR bursts on the other hand show no correlation with pulse phase. Palmer (2002) found that hundreds of bursts from SGR 1900+14 were distributed uniformly in phase. However as discussed by Gavriil et al. (2004), Woods et al. (2005) and below, this is not the only difference between SGR and AXP bursts.

If AXP bursts do occur at specific pulse phases then they must be associated with particularly active regions of the star. This would imply that AXPs burst much more frequently than is observed, but the bursts go unseen because they are beamed away from us. However, even if a burst is missed, it may still leave two characteristic signatures. One is a very long tail: those observed in 1E 1048.1–5937 and XTE J1810–197 lasted several pulse cycles. Second, short-term increases in pulsed flux like those observed in this paper would be an indication of a burst whose onset went unobserved. A search for “naked tails” or short time scale pulsed flux enhancements could in principle demonstrate the existence of missed bursts.

The very long tail (> 699 s) of the burst reported here makes it very similar to one burst observed from 1E 1048.1–5937, some of the bursts seen in AXP 1E 2259+586, and to those observed in XTE J1810–197. Their long durations set these bursts apart from the brief ~ 0.1 s burst observed in SGRs. As argued by Woods et al. (2005), bursts from 1E 1048.1–5937 XTE J1810–197 and 1E 2259+586, which have very long tails and occur close to pulse maximum, might constitute a new class of bursts unique to AXPs. Although there were two

bursts with extended tails observed from SGR 1900+14, many of their properties differ from those of the long-duration AXP bursts. The first extended-tail SGR burst occurred on 1998 April 29 (Ibrahim et al. 2001) and the second on 2001 April 28 (Lenters et al. 2003). In both cases an obvious distinction could be made between the initial “spike” and the extended “tail” component of the burst. For the AXP bursts which have a fast rise and smooth exponential decay morphology, there is no point which clearly marks the transition between initial spike and extend tail. Furthermore in both of these extended-tail SGR bursts, the majority of the energy was in the initial spike, not the tail. In fact, from the time of their peaks to $\sim 1\%$ of their total duration, $\sim 98\%$ of their total energy was released. By contrast, in the AXP bursts, virtually all the energy is in what would be considered the tail component. For the burst reported here, from the time of its peak to $\sim 1\%$ of its total duration $< 37\%$ of its total energy was released. Also, unlike the long-duration AXP bursts which all occurred near pulse maximum, the extended-tail SGR bursts occurred 180° apart in pulse phase, i.e., the first burst occurred near pulse maximum and the second burst near pulse minimum (Lenters et al. 2003). Last, the long-tailed SGR bursts only occurred following high-luminosity flares: the first followed the 1998 August 27 SGR 1900+14 event and the second followed the 2001 April 18 event (Guidorzi et al. 2001). No such high-luminosity flares have ever been observed in an AXP.

From its earliest stages, the magnetar model put forward by Thompson & Duncan (1995) offered a viable burst mechanism for SGRs and AXPs. In a magnetar, the magnetic field is strong enough to crack the crust of the neutron star. The fracturing of the crust disturbs the magnetic field foot-points and releases an electron-positron-photon fireball into the magnetosphere. The fireball is trapped and suspended above the fracture site by closed field lines. The suspended fireball heats the surface, and in the initial version of this model, it was suggested that the burst duration would be comparable to the cooling time. In more recent work it has been suggested that burst durations can be extended by orders of magnitude via vertical expansion of the surface layers (Thompson et al. 2002) or deep crustal heating (Lyubarsky et al. 2002). The surface fracture mechanism can explain the very long durations of the bursts observed from 1E 1048.1–5937 and XTE J1810–197. Furthermore this mechanism also provides an explanation for the phase dependence of the AXP bursts, since the fracture sites are thought to be preferentially located near the magnetic poles. Hence the bursts would be associated with a particular active region on the surface, resulting in a correlation with pulse phase.

Lyutikov (2002) proposed another burst emission mechanism within the framework of the magnetar model. He suggested that the bursting activity of AXPs and SGRs is due to the release of magnetic energy stored in non-potential magnetic fields by reconnection-type events in the magnetosphere. In this model, bursts occur at random phases because the

emission site is high in the magnetosphere. Hence we observe all bursts. This mechanism will produce harder and shorter bursts as compared to the ones due to surface fracturing. Softer and longer bursts are achieved by a combination of reconnection and a small contribution from surface cooling, as energetic reconnection events will precipitate particles which will heat the surface. Since there is a duration-fluence correlation in both SGR (Gögüş et al. 2001) and AXP (Gavriil et al. 2004) bursts, this model suggests that the shorter (less-luminous) bursts are harder than the longer (more luminous) bursts. A hardness-fluence correlation was found for SGR bursts (Gögüş et al. 2001), but an anti-correlation was found for the 80 bursts from AXP 1E 2259+586 (Gavriil et al. 2004). It should also be noted that for 1E 1048.1–5937 and XTE J1810–197 the more energetic bursts are the hardest, although only three bursts have been observed thus far. Hence the aspects that differentiate the surface-cooling model from the reconnection model for bursts seem to be the same aspects that separate the canonical SGR bursts from the long-duration AXP bursts. In the surface-cooling model one expects longer durations, a correlation with pulse phase and a fluence-hardness anti-correlation.

It is possible that both mechanisms (surface and magnetospheric) are responsible for creating AXP and SGR bursts, but that magnetospheric bursts are more common in SGRs. This is not unreasonable if we consider the twisted-magnetosphere model proposed by Thompson et al. (2002). In this extension to the magnetar model, Thompson et al. (2002) suggested that the highly twisted internal magnetic field of a magnetar imposes stresses on the crust which in turn twist the external dipole field. The twisted external fields induce large-scale currents in the magnetosphere. The inferred dipole magnetic field strengths, luminosity and spectra of SGRs all suggest that the global “twists” of their magnetic fields are greater than those of the AXPs. If the external fields of SGRs are much more “twisted” than those of the AXPs, that would make them more susceptible to reconnection type events in their magnetosphere. Furthermore, if SGRs have stronger magnetic fields than the AXPs, then they would be less susceptible to surface fracture events because at high field strengths the crustal motions are expected to become plastic.

What could make a burst tail last longer in AXPs? One possibility is that the energy is released very deep in the crust and the energy conducts to the surface on very long time scales. In this scenario most of the heat is absorbed by the core, which could explain why AXP bursts are in general dimmer than SGR bursts. In order for this model to explain both the extended-tail SGR bursts and the long-duration AXP bursts one can imagine a hybrid scenario in which a sudden twist occurs, which deposits energy both in the magnetosphere and deep in the crust. The energy deposited in the magnetosphere gives rise to a spike and the energy deposited deep in the crust conducts to the surface on longer time scales. The reason why no spike is seen in the AXPs is because the magnetospheric component is small. This reasoning applies to AXPs 1E 1048.1–5937 and XTE J1810–197 but it is not

surprising that AXP 1E 2259+586 exhibits both types of bursts, because as argued by Woods et al. (2004) the best explanation for the bursts and contemporaneous flux, pulse profile and spin-down variability from this source was through a catastrophic event that simultaneously impacted the interior and the magnetosphere of the star.

The spectrum of the burst reported here is intriguing. First, although this burst is much harder given its luminosity when compared to SGR bursts (the SGRs show a luminosity-hardness anti-correlation), its spectral softening is very similar to those of the extended-tail bursts of SGR 1900+14 (Ibrahim et al. 2001; Lenters et al. 2003). Second, the evidence of a spectral feature at ~ 13 keV makes this burst very similar to the first burst detected from 1E 1048.1–5937 (Gavriil et al. 2002). The probability of observing an emission line at ~ 13 keV in both bursts is exceedingly small, thus the line is almost certainly intrinsic to the source and has important implications. If it is a proton-cyclotron line then it allows us to calculate the surface magnetic field strength, $B = m_p c E / \hbar e = 2.1 \times 10^{15} (E/13 \text{ keV})$ G, where m_p and e are the proton mass and charge, respectively, and E is the energy of the feature. This value for the magnetic field strength is greater than that measured from the spin-down of the source, but the spin-down is only sensitive to the dipolar component of the field and it is plausible that the field is multipolar. It should be noted that this surface magnetic field strength estimation assumes the burst was a surface cracking phenomenon. An open question is why bursts from certain magnetar candidates exhibit spectral features and others do not. 1E 2259+586 exhibited over 80 bursts and no spectral features were seen, whereas 1E 1048.1–5937 showed only three bursts with 2 spectral features seen. Woods et al. (2005) reported a spectral feature at approximately the same energy in a burst from AXP XTE J1810–197 at a higher significance level than both of the 1E 1048.1–5937 spectral features.

We have argued that the bursts from 1E 1048.1–5937 are very similar to those of XTE J1810–197. Interestingly, the two sources show other similarities. They both have sinusoidal profiles while all other AXPs exhibit rich harmonic content in their pulse profiles (see Gavriil & Kaspi 2002; Gotthelf et al. 2002). They have shown long-lived ($>$ months) pulsed flux variations which are not due to cooling of the crust after the impulsive injection of heat from bursts. Furthermore, their timing properties are the most reminiscent of the SGRs.

The pulsed fraction decrease we have observed lends further evidence that the pulsed flux variations observed by Gavriil & Kaspi (2004) represent a new phenomenon seen exclusively in the AXPs. The fact that the pulsed fraction decreased as the pulsed flux increased without any pulse morphology changes implies that there was a greater fractional increase in the unpulsed flux than in the pulsed flux, in agreement with what was found by Mereghetti

et al. (2004). Such a flux enhancement cannot be attributed to a particular active region. Thus we can rule out the flux enhancements were due to the injection of heat from bursts that were beamed away from us, because in that scenario one would expect a larger fractional change in pulsed flux than in total flux. Indeed, during the burst afterglow pulsed flux enhancement in SGR 1900+14, Lenters et al. (2003) found a pulsed flux and pulse fraction increase.

4. Conclusions

We reported on the discovery of the latest burst from the direction of AXP 1E 1048.1–5937. This burst was discovered as part of our long-term monitoring campaign of AXPs with *RXTE*. Contemporaneously with the burst we discovered a pulsed-flux enhancement which unambiguously identified 1E 1048.1–5937 as the burst’s origin. The clear identification of 1E 1048.1–5937 as the burster in this case argues that it was indeed the emitter of the two bursts discovered from the direction of this source in 2001, as already inferred by Gavriil et al. (2002).

All three bursts from 1E 1048.1–5937 can only be explained within the context of the magnetar model, however many of their properties differentiate them from canonical SGR bursts. This and the first burst discovered from this source had very long-tails, > 699 s and ~ 51 s respectively, as opposed to the ~ 0.1 s duration SGR bursts. Two ks-long SGR bursts have been reported but we argued that they were a very different phenomenon (Ibrahim et al. 2001; Lenters et al. 2003). Specifically the extended-tail SGR bursts had very energetic initial spikes and the long tails were argued to be the afterglow of this initial injection of energy. However, in the AXP bursts no such spikes are present; in fact, most of the energy is in what would be considered the tail. All three bursts from 1E 1048.1–5937 occurred near pulse maximum, as opposed to the SGR bursts which are uniformly distributed in pulse phase. All of the bursts discovered from AXP XTE J1810–197 and a handful of the bursts from AXP 1E 2259+586 share many properties with the 1E 1048.1–5937 bursts and, as argued by Woods et al. (2005), long-tailed bursts (with no energetic spikes) which occur near pulse maxima might comprise an new burst class thus far unique to AXPs.

The spectral evolution of this burst was very similar to the extended-tail SGR bursts with the trend going from hard to soft. However, at one part of the bursts tail there was an unusual spectral feature at ~ 13 keV; a similar feature was discovered in the first burst from 1E 1048.1–5937 and in a very high signal-to-noise burst from XTE J1810–197 (Gavriil et al. 2002; Woods et al. 2005). If features such as these are confirmed they may provide direct estimates of the neutron star’s magnetic field especially if harmonic features can be

positively identified.

The differences between the long- and short-duration bursts might be due to separate emission mechanisms. Two burst mechanisms have been proposed within the magnetar model: surface fracture and magnetospheric reconnection (Thompson & Duncan 1995; Lyutikov 2002). We argued that this burst is more likely a surface fracture event which agrees with the conclusion reached by Woods et al. (2005) for the long-tailed bursts from XTE J1810–197. If in fact the two classes of bursts are due to emission mechanisms operating in two distinct regions (near the surface and in the upper magnetosphere), then AXP bursts provide opportunities to probe the physics of these separate regions of a magnetar.

We are very grateful to Maxim Lyutikov for valuable comments, suggestions and useful discussion. This work is supported from NSERC Discovery Grant 228738-03, NSERC Steacie Supplement 268264-03, a Canada Foundation for Innovation New Opportunities Grant, FQRNT Team and Centre Grants, the Canadian Institute for advanced Research, SAO grant GO4-5162X and NASA grant NNG05GA54G. V.M.K. is a Canada Research Chair and Steacie Fellow. This research has made use of data obtained through the High Energy Astrophysics Science Archive Research Center Online Service, provided by the NASA/Goddard Space Flight Center.

REFERENCES

- Gögüş, E., Kouveliotou, C., Woods, P. M., Thompson, C., Duncan, R. C., & Briggs, M. S. 2001, *ApJ*, 558, 228
- Gavriil, F. P. & Kaspi, V. M. 2002, *ApJ*, 567, 1067
- Gavriil, F. P. & Kaspi, V. M. 2004, *ApJ*, 609, L67
- Gavriil, F. P., Kaspi, V. M., & Woods, P. M. 2002, *Nature*, 419, 142
- . 2004, *ApJ*, 607, 959
- Gotthelf, E. V., Gavriil, F. P., Kaspi, V. M., Vasisht, G., & Chakrabarty, D. 2002, *ApJ*, 564, L31
- Guidorzi, C., Montanari, E., Frontera, F., Costa, E., Gandolfi, G., Feroci, M., Piro, L., Amati, L., in't Zand, J. J. M., D'Andreta, G., Kaptein, R., & Reboa, L. 2001, *GRB Circular Network*, 1041, 1

- Hurley, K., Cline, T., Mazets, E., Barthelmy, S., Butterworth, P., Marshall, F., Palmer, D., Aptekar, R., Golenetskii, S., Ill'inski, V., Frederiks, D., McTiernan, J., Gold, R., & Trombka, T. 1999, *Nature*, 397, 41
- Ibrahim, A. I., Safi-Harb, S., Swank, J. H., Parke, W., Zane, S., & Turolla, R. 2002, *ApJ*, 574, L51
- Ibrahim, A. I., Strohmayer, T. E., Woods, P. M., Kouveliotou, C., Thompson, C., Duncan, R. C., Dieters, S., Swank, J. H., van Paradijs, J., & Finger, M. 2001, *ApJ*, 558, 237
- Ibrahim, A. I., Swank, J. H., & Parke, W. 2003, *ApJ*, 584, L17
- Israel, G. L., Covino, S., Stella, L., Campana, S., Marconi, G., Mereghetti, S., Mignani, R., Negueruela, I., Oosterbroek, T., Parmar, A. N., Burderi, L., & Angelini, L. 2002, *ApJ*, 580, L143
- Jahoda, K., Swank, J. H., Giles, A. B., Stark, M. J., Strohmayer, T., Zhang, W., & Morgan, E. H. 1996, *Proc. SPIE*, 2808, 59
- Kaspi, V. M., Chakrabarty, D., & Steinberger, J. 1999, *ApJ*, 525, L33
- Kaspi, V. M., Gavriil, F. P., Chakrabarty, D., Lackey, J. R., & Munro, M. P. 2001, *ApJ*, 558, 253
- Kaspi, V. M., Gavriil, F. P., Woods, P. M., Jensen, J. B., Roberts, M. S. E., & Chakrabarty, D. 2003, *ApJ*, 588, L93
- Kaspi, V. M., Lackey, J. R., & Chakrabarty, D. 2000, *ApJ*, 537, L31
- Kouveliotou, C., Dieters, S., Strohmayer, T., van Paradijs, J., Fishman, G. J., Meegan, C. A., Hurley, K., Kommers, J., Smith, I., Frail, D., & Murakami, T. 1998, *Nature*, 393, 235
- Kouveliotou, C., Strohmayer, T., Hurley, K., Van Paradijs, J., Finger, M. H., Dieters, S., Woods, P., Thompson, C., & Duncan, R. C. 1999, *ApJ*, 510, L115
- Lenters, G. T., Woods, P. M., Goupell, J. E., Kouveliotou, C., Göğüs, E., Hurley, K., Frederiks, D., Golenetskii, S., & Swank, J. 2003, *ApJ*, in press
- Lyubarsky, Y., Eichler, D., & Thompson, C. 2002, *ApJ*, 580, L69
- Lyutikov, M. 2002, *ApJ*, 580, L65

- Mazets, E. P., Golenetskii, S. V., Il'inskii, V. N., Apetkar', R. L., & Gur'yan, Y. A. 1979, *Nature*, 282, 587
- Mereghetti, S., Tiengo, A., Stella, L., Israel, G. L., Rea, N., Zane, S., & Oosterbroek, T. 2004, *ApJ*, 608, 427
- Palmer, D. M. 2002, *Memorie della Societa Astronomica Italiana*, 73, 578
- Strohmayer, T. E. & Ibrahim, A. I. 2000, *ApJ*, 537, L111
- Thompson, C. & Duncan, R. C. 1995, *MNRAS*, 275, 255
- Thompson, C. & Duncan, R. C. 1996, *ApJ*, 473, 322
- Thompson, C., Lyutikov, M., & Kulkarni, S. R. 2002, *ApJ*, 574, 332
- Woods, P. M., Kaspi, V. M., Thompson, C., Gavriil, F. P., Marshall, H. L., Chakrabarty, D., Flanagan, K., Heyl, J., & Hernquist, L. 2004, *ApJ*, 605, 378
- Woods, P. M., Kouveliotou, C., Gavriil, F. P., Kaspi, M., V., Roberts, M. S. E., Ibrahim, A., Markwardt, C. B., Swank, J. H., & Finger, M. H. 2005, *ApJ*, in press
- Woods, P. M. & Thompson, C. 2004, in *Compact Stellar X-ray Sources*, ed. W. H. G. Lewin & M. van der Klis (UK: Cambridge University Press), in press (astro-ph/0406133)

Table 1. Burst Timing and Spectral Properties

Temporal Properties	
Burst day, (MJD)	53185
Burst start time, (UT)	6:52:33.63(18)
Burst rise time, t_r (ms)	$18.2^{+5.8}_{-4.4}$
Burst duration, T_{90} (s)	> 699
Burst phase	-0.078 ± 0.016
Fluxes and Fluences	
T_{90} fluence ^a (counts)	> 5387
T_{90} fluence ^a ($\times 10^{-10}$ erg cm ⁻²)	> 330
Peak flux for 64 ms ^a ($\times 10^{-10}$ erg s ⁻¹ cm ⁻²)	59 ± 9
Peak flux for t_r ms ^a ($\times 10^{-10}$ erg s ⁻¹ cm ⁻²)	105 ± 20
Spectral Properties	
<u>Power law:</u>	
Power law index	$1.06^{+0.14}_{-0.12}$
Power law flux ($\times 10^{-11}$ erg s ⁻¹ cm ⁻²)	2.6 ± 0.9
Reduced χ^2 /degrees of freedom	1.00/62
<u>Blackbody:</u>	
kT (keV)	$2.99^{+0.25}_{-0.23}$
Blackbody flux ($\times 10^{-11}$ erg s ⁻¹ cm ⁻²)	2.4 ± 0.3
Reduced χ^2 /degrees of freedom	0.78/62

^aFluxes and fluences calculated in the 2–20 keV band.

Table 2. Phase-averaged spectral fit parameters and pulsed fractions of 1E 1048.1–5937.

Parameter ^a	July 8	July 10	July 15
N_H (10^{22} cm ⁻²)	1.18(4)	1.18(4)	1.23(5)
kT (keV)	0.619(14)	0.585(12)	0.585(12)
Γ	3.30(9)	3.08(11)	3.23(12)
Flux ^b (10^{-12} ergs cm ⁻² s ⁻¹)	7.51	7.91	7.51
Unabs Flux ^c (10^{-12} ergs cm ⁻² s ⁻¹)	9.07	9.56	9.20
χ^2/dof	307/306	293/286	306/278
Pulsed Fraction ^d	0.561(7)	0.563(9)	0.551(10)

^aNumbers in parentheses indicate the 1σ uncertainty in the least significant digits of the spectral parameter. Note that these uncertainties reflect the 1σ error for a reduced χ^2 of unity.

^bObserved flux from both spectral components 2–10 keV.

^cUnabsorbed flux from both spectral components 2–10 keV.

^dRms pulsed fraction (2.0–10.0 keV) following the definition in Woods et al. (2004).

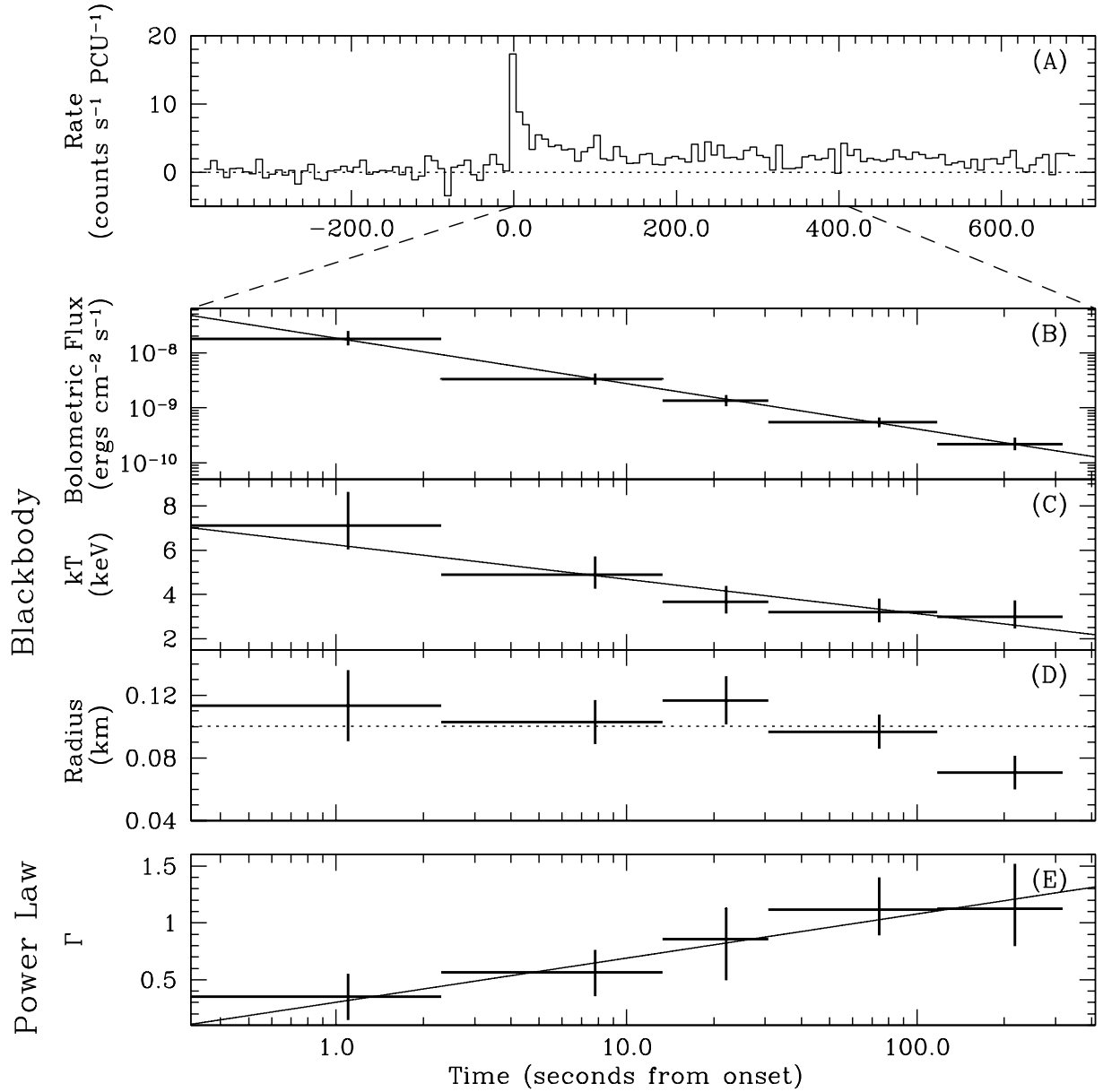


Fig. 1.— A: Background subtracted burst time series in the 2–20 keV band binned with 8-s time resolution. B: Bolometric flux (F) time series. The line represents the best-fit power law, $F = 1.84 \times 10^{-8}(t/1 \text{ s})^{-0.82} \text{ erg cm}^{-2} \text{ s}^{-1}$. C: Blackbody temperature (kT) time series. The line represents the best-fit logarithmic function, $kT = 6.24 - 1.55 \log(t/1 \text{ s}) \text{ keV}$. D: Blackbody radius versus time. The dotted line represents the average emission radius, $R = 0.10 \text{ km}$ assuming a distance of 5 kpc. E: Power-law index (Γ) time series. The line represents the best-fit logarithmic function, $\Gamma = 0.30 + 0.39 \log(t/1 \text{ s})$.

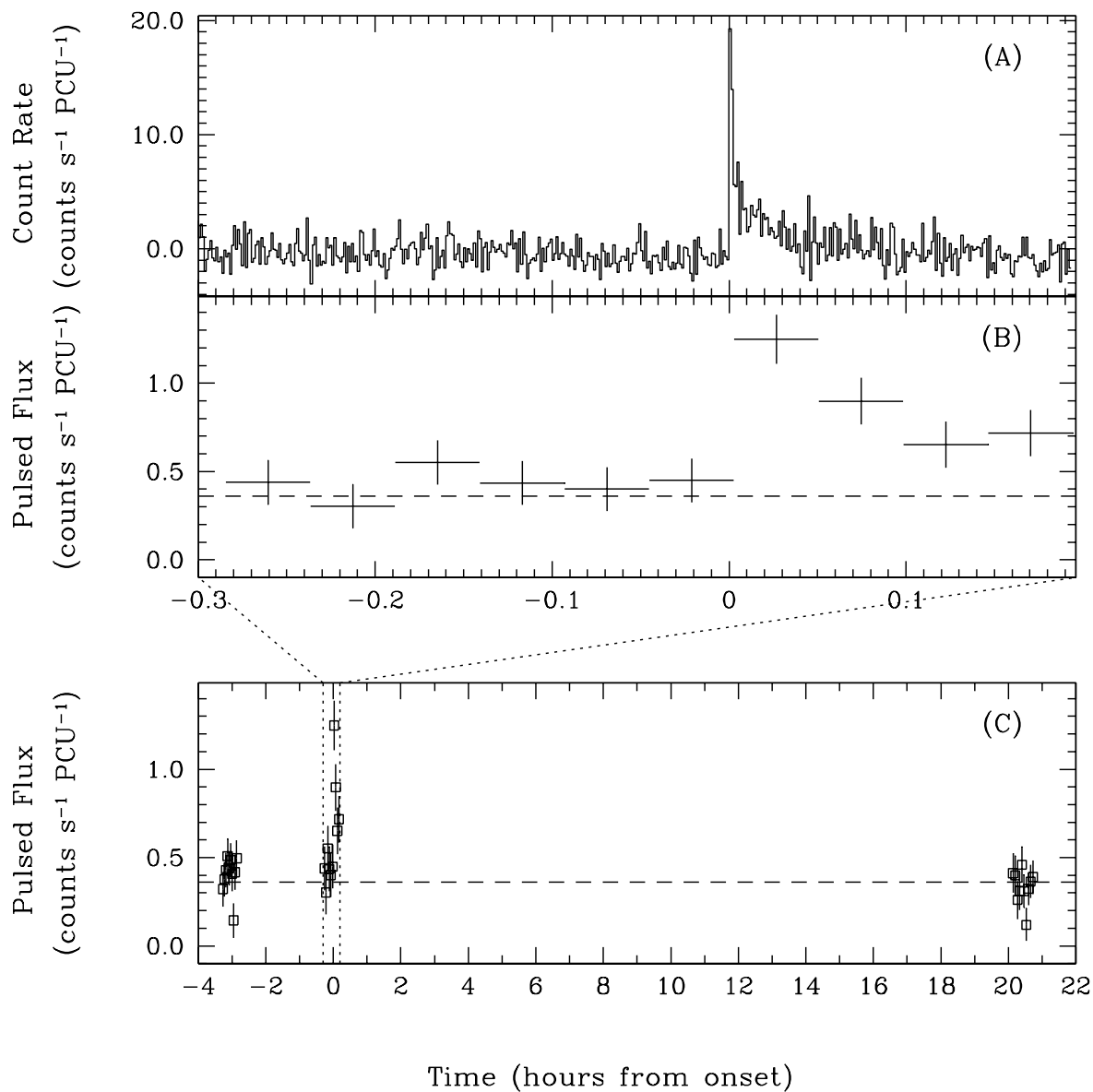


Fig. 2.— A: Burst time series in the 2–20 keV band, binned with 4-s time resolution. B: Pulsed flux in the 2–10 keV band during the observation. The dashed line represents the average *quiescent* pulsed flux as measured from neighboring observations. C: Same as above except for a longer baseline.

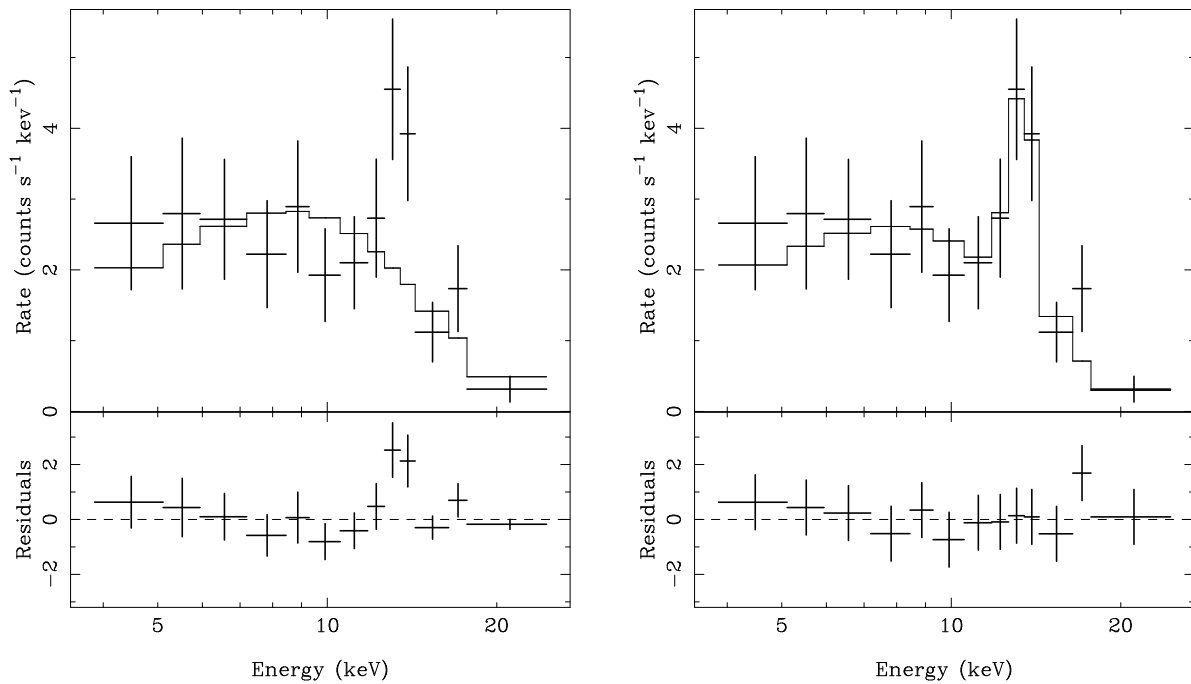


Fig. 3.— Left: An 8-s long spectrum starting 1 s after the peak of the burst fit with a simple blackbody model. The fit had $\chi_{\text{dof}} = 1.6$ for 11 degrees of freedom. There is a possibility of a spectral feature at ~ 13 keV. Right: The same spectrum as on the left, but fit with a blackbody plus a Gaussian emission line. The fit had $\chi_{\text{dof}} = 0.6$ for 8 degrees of freedom.

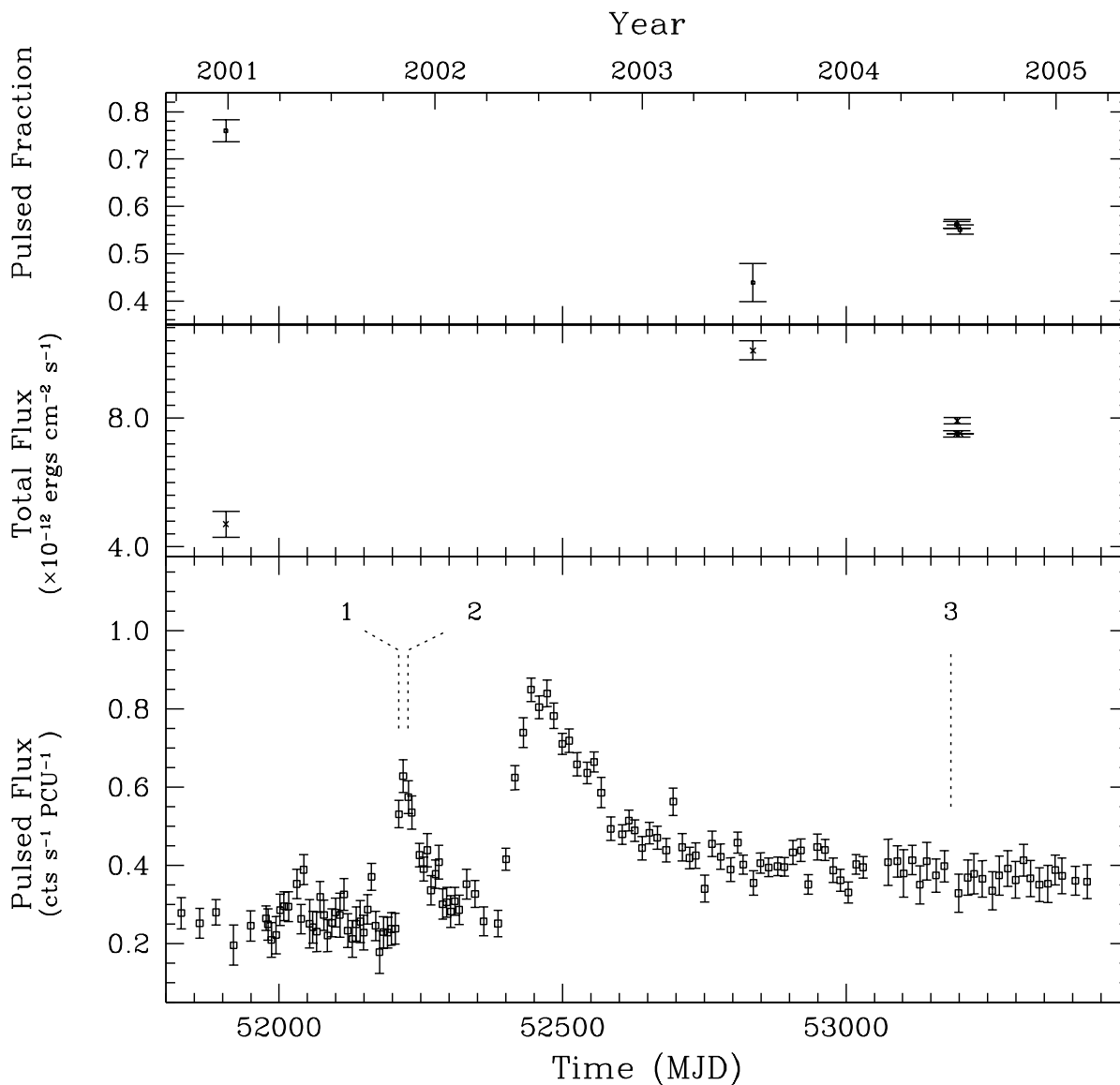


Fig. 4.— 1E 1048.1–5937’s total and pulsed flux evolution. Top: 2–10 keV pulsed fraction as measured by *XMM-Newton* and *Chandra* (see Woods et al. 2004, for our particular definition of pulsed fraction). Middle: 2–10 keV total flux as measured by *XMM-Newton* and *Chandra*. Bottom: 2–10 keV pulsed flux as measured by *RXTE* (for details on the analysis see Gavriil & Kaspi 2004). The epochs of the three bursts observed from 1E 1048.1–5937 are indicated by their respective numbers.